Multichannel-quantum-defect-theory treatment of preionized and predissociated triplet gerade levels of H_2

A. Matzkin,[1,*] Ch. Jungen, and S. C. Ross[1,2]
[1]*Laboratoire Aimé Cotton, CNRS, Université de Paris–Sud, 91405 Orsay, France*
[2]*Department of Physics, University of New Brunswick, P.O. Box 4400, Fredericton, New Brunswick, Canada E3B 5A3*
(Received 7 April 2000; published 15 November 2000)

Multichannel quantum defect theory (MQDT) is used to calculate highly excited predissociated and preionized triplet gerade states of H_2. The treatment is *ab initio* and is based on the clamped-nuclei quantum-defect matrices and dipole transition moments derived from quantum-chemical potential energy curves by Ross *et al.* [Can. J. Phys. (to be published)]. Level positions, predissociation or preionization widths and relative intensities are found to be in good agreement with those observed by Lembo *et al.* [Phys. Rev. A **38**, 3447 (1988); J. Chem. Phys. **92**, 2219 (1990)] by an optical-optical double resonance photoionization or depletion technique.

PACS number(s): 31.15.−p, 33.80.Gj, 33.80.Eh, 34.50.Gb

I. INTRODUCTION

Highly excited triplet states of H_2 have been observed in optical emission in discharges since the early work of Richardson [1] and Dieke [2]. However, it was not until 1983 that Eyler and Pipkin [3] who produced excited triplet H_2 by electron bombardment, were able to carry out high-resolution laser studies of excited triplet gerade bound (and weakly predissociated) levels arising from the $4s$ and $4d$ Rydberg orbitals. More recently, Bjerre *et al.* [4] and Lembo *et al.* [5,6] used the charge exchange reaction of H_2^+ ions with Cs atoms to populate various vibrational-rotational levels of the metastable $c\ ^3\Pi_u^-$ state of H_2. Laser excitation of these long-lived levels then leads to strongly predissociated and preionized triplet gerade states at higher energies than were reached in the preceding experiments. Since in these experiments the vibrational-rotational population distribution in the lower c state was unknown and could not be controlled, an optical-optical double-resonance depletion technique was employed that permitted the singling out of spectral resonances originating from a common lower level. In this way most of the bound lower levels $c\ ^3\Pi_u^-$, v'', N'' of the observed resonances could be assigned with confidence and tentative assignments of the upper-state values N (and parity) could also be given. By using a variant of the depletion technique, Lembo *et al.* [5] detected a progression of broad resonances which, while lying above the ionization as well as the $H(1s)+H(n=2)$ dissociation threshold, turned out to decay only into the molecular dissociation channel. These resonances were assigned to the $j\ ^3\Delta_g^-$ state predissociated by the $i\ ^3\Pi_g^-$ state. This is illustrated schematically by Fig. 1, which displays selected potential-energy curves of triplet H_2 in the energy range relevant for these experiments. Their assignments were based on the agreement, to within about 10 cm^{-1}, of the positions of the observed resonances and theoretical bound vibrational levels calculated for the j state with the best available *ab initio* potential-energy curve [7].

In another set of experiments, Lembo *et al.* [6] found sharper resonances ($\Gamma \approx 1-4\ cm^{-1}$) that are simultaneously preionized and predissociated and where the competition between the two decay channels varies from one resonance to another. These upper states could only tentatively be associated with the predicted $r\ ^3\Pi_g$ state of H_2 but no detailed interpretation was given.

The aim of the present work is to present a unified interpretation of the experiments of Bjerre, Helm and, collaborators in terms of multichannel quantum-defect theory using the clamped-nuclei quantum-defect matrices derived in Ref. [8]. We confirm essentially all assignments and conclusions of Refs. [4–6]. In addition, we are able to assign some of the spectral features that previously could not be attributed, and we account quantitatively for most aspects of their observations including resonance positions, resonance profiles and the competition between ionization and dissociation.

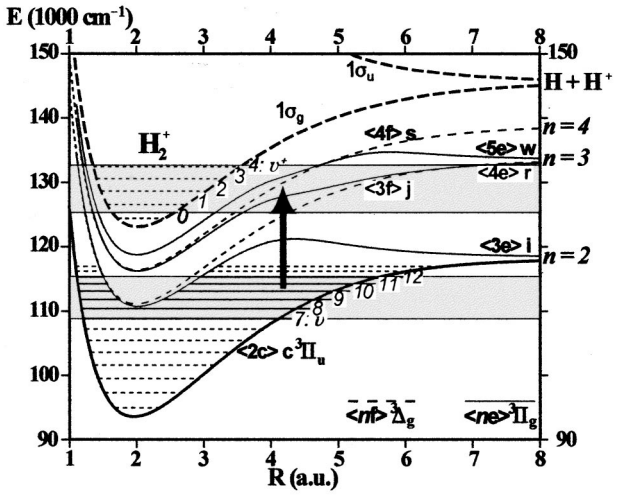

FIG. 1. Selected potential-energy curves of triplet H_2 (full lines, $^3\Pi_g$; thin dashed lines, $^3\Delta_g$) and H_2^+ (thick dashed lines). The excitation scheme is indicated by a vertical arrow. The ranges of lower and upper levels involved in the experiments of Refs. [4–6] are indicated by pairs of horizontal lines, respectively.

*Present address: Department of Physics and Astronomy, University College London, Gower Street, WC1E 6BT London, Great Britain.

II. THEORY

In this section, we present a brief review of a treatment of competing molecular ionization and dissociation processes that is unified in the sense that the radial coordinate of the Rydberg electron r, and the dissociative reaction coordinate R are treated on the same footing. Thus the concept of the ''molecular core'' is extended accordingly: It is defined by $r<r_0$, $R<R_0$, where r_0 corresponds to the range of the multipole and polarization long-range fields of the H_2^+ core, and R_0 corresponds, roughly, to the range of the molecular electronic ground- and excited-state potentials of H_2^+. Apart from its conceptual appeal, one advantage of our approach is that the coupling of ionization and dissociation channels is treated nonperturbatively.

A stationary wave function allowing for both ionization and dissociation can be set up as follows: Outside the core $(r>r_0)$ one writes

$$\psi^\rho(r)=\sum_{i\in\{I_0+I_c\}}|i\rangle\left\{Z_i^\rho f_i(r)-\left[\sum_{i'}Z_{i'}^\rho K_{i',i}^{II}+\sum_{d'}Z_{d'}^\rho K_{d',i}^{DI}\right]g_i(r)\right\},\qquad(1)$$

Here, f_i and g_i are, respectively, regular (sin-type) and irregular (cos-type) radial Coulomb wave functions appropriate for the Coulomb interaction $V_i(r)=-2/r+l_i(l_i+1)/r^2$ (in Rydberg units) between the separating H_2^+ core and e^- Rydberg electron. $|i\rangle$ denotes the rovibronic core state e^+, v_e^+, N_e^+ together with the angular part l_i of the Rydberg electron wave function. $K_{i',i}^{II}$ and $K_{d',i}^{ID}$ are reaction matrix elements connecting different ionization channels or ionization channels with dissociation channels, respectively. Z are channel expansion coefficients and ρ is a solution index. For $R>R_0$, the analog of Eq. (1) is given by

$$\psi^\rho(R)=\sum_{d\in\{D_0\}}|d\rangle\left\{Z_d^\rho F_d(R)-\left[\sum_{d'}Z_{d'}^\rho K_{d',d}^{DD}+\sum_{i'}Z_{i'}^\rho K_{i',d}^{ID}\right]G_d(R)\right\},\qquad(2)$$

where, for example, $F_d(R)$ and $G_d(R)$ are taken to be regular and irregular free-particle vibrational continuum functions, respectively. K^{DD} is due to the interaction $V_d(R)=U_d(R)+J_d(J_d+1)/\mu R^2$ (U_d is the Born-Oppenheimer potential, μ is the reduced nuclear mass) between two separating H atoms. $|d\rangle$ denotes the corresponding molecular electronic state, together with the angular (rotational) part J_d of the separating H atoms. Equations (1) and (2) are stationary multichannel scattering wave functions. Note that the summation in Eq. (1) includes open as well as closed channels as is characteristic for multichannel quantum-defect theory where long-range Rydberg states are treated on the same footing as ionization scattering states. In Eq. (2), on the other hand, we have omitted the summation over long-range bound vibrational states since such states (arising, e.g., from H^++H^- ion-pair states) do not occur in the present problem. Our task at this point is to evaluate the matrices K^{II}, K^{DD} and K^{ID} for the problem at hand. Their direct calculation by *ab initio* theory has been discussed recently by one of us [9], but is not feasible at this stage for the present problem. Instead, we shall follow the procedure outlined in Ref. [10] where it was shown how wave functions of the form in Eqs. (1) and (2) can be related to the clamped-nuclei purely electronic quantum-defect matrices.

In the absence of coupling between I and D, the submatrix K^{II} may be calculated from the clamped-nuclei quantum defects by the well-known procedures of molecular MQDT combined with rotational-vibrational frame transformations (see various papers reprinted in Ref. [11]), while K^{DD} is taken diagonal since dissociation is assumed to take place separately along the relevant Born-Oppenheimer potential-energy curves. The procedure [10] for evaluating K^{ID} starts out by writing Eqs. (1) and (2) in eigenchannel form, e.g., for dissociation:

$$\psi^\rho(R)=\sum_{d\in\{D_0\}}T_{d,\rho}|d\rangle[F_d(R)-\tan(\pi\tau_\rho)G_d(R)],\qquad(3)$$

where the $T_{d,\rho}$ are the elements of the unitary projection matrix T that diagonalizes the open-channel interaction (I and D). The fact that K^{ID} is present introduces an additional contribution to the asymptotic phase shift $\pi\tau_\rho$ that would not be there if $K^{ID}=0$. This additional phase shift changes the logarithmic derivative of the vibrational component at $R=R_0$, $-b$, with respect to what it would have been. The procedure first performs a few (two or three typically) initial calculations with ''trial'' values of b or, in other words, with arbitrary assumed K^{ID}. The superposition principle is then used to obtain the correct K^{ID} that yields identical eigenphases $\pi\tau_\rho$ in all channels I and D. For an initial fixed trial value of b at $R=R_0$, Eq. (2) takes the form

$$\psi^{\rho(x)}(R)=\sum_{d\in\{D_0\}}Z_d^{\rho(x)}|d\rangle[F_d(R)-\tan(\pi\tau_d^{(x)})G_d(R)],\qquad(4)$$

where $x=1,2...$ refers to the calculation carried out with the logarithmic derivative $-b^{(x)}$. The channel mixing coefficients $Z_d^{\rho(x)}$ are determined by carrying out a ''normal'' rovibronic MQDT calculation for $R\leqslant R_0$, expressed in terms of the clamped-nuclei quantum-defect matrices $\mu^{(\Lambda)}(R)$. In this calculation, each vibrational basis function $\chi(R\leqslant R_0)$ has the same $b^{(x)}$ value at $R=R_0$ and the continuous connection with the asymptotic form of [Eq. (4)] is thus ensured. The frame transformation procedure in turn connects $\psi^{\rho(x)}$ to the I arrangement. For large r, where the closed-channel components of Eq. (1) are vanishing exponentially, one obtains

$$\psi^{\rho(x)}(r)=\sum_{i\in\{I_0\}}Z_i^{\rho(x)}|i\rangle[f_i(r)-\tan(\pi\tau_\rho^{(x)})g_i(r)],\qquad(5)$$

where ρ takes the values $1...N_{I_0}$ with N_{I_0} the number of open ionization channels. At this point we have constructed a total

wave function of eigenchannel form, but this will have dissociation phase shifts $\pi\tau_d^{(x)}$ in the D arrangement that in general differ from the $\pi\tau_\rho^{(x)}$'s obtained for the I arrangement. In addition, the Z_d^ρ and Z_i^ρ coefficients will not form a unitary matrix contrary to what is expected according to Eq. (3).

We now make use of the fact that any desired phase shift in a given dissociation channel d can be obtained by a superposition of two functions $\psi^{\rho(x)}$, $x=1,2$, with suitable coefficients $c^{\rho(x)}$. The following combination will generate a common asymptotic phase shift in all channels i and d:

$$\sum_{\rho(x)} c^{\rho(x)\psi^{\rho(x)}}(r) = \sum_{i\in I_0} |i\rangle Z_i^\rho [f_i(r) - \tan(\pi\tau_\rho) g_i(r)], \tag{6a}$$

$$\sum_{\rho(x)} c^{\rho(x)\psi^{\rho(x)}}(R) = \sum_{d\in D_0} |d\rangle Z_d^\rho [F_d(R) - \tan(\pi\tau_\rho) G_d(R)], \tag{6b}$$

Since our system has in all $N_{I_0}+N_{D_0}$ open channels, we need the same number of superposition coefficients $c^{\rho(x)}$. In order to have the correct number of Eqs. (6) we may thus e.g., take all the N_{I_0} solutions for $x=1$ and select N_{D_0} solutions from the set $x=2$. By replacing $\psi^{\rho(x)}(r)$ and $\psi^{\rho(x)}(R)$ in Eq. (6) by their asymptotic expressions (4) and (5), (with coefficients Z and phase shifts τ already known) we obtain a generalized linear eigenvalue system whose solution yields the coefficients c and the eigenphases $\pi\tau$. With these quantities known, we evaluate the channel coefficients Z_i^ρ and Z_d^ρ: these are in fact the elements $T_{i,\rho}$ and $T_{d,\rho}$ of the $(N_{I_0}+N_{D_0})\times(N_{I_0}+N_{D_0})$ unitary eigenvector matrix of the total reaction matrix K consisting of K_{II}, K_{DD}, and K_{ID}.

This procedure thus relates the total reaction matrix K to the known body-fixed quantum-defect matrices $\mu^{(\Lambda)}(R)$. In order to account for the laser experiments we also require the dipole transition amplitudes for excitation from the c state to the triplet gerade channels. The superposition and transformation coefficients determined in the various stages of the evaluation of K similarly relate the desired effective real dipole transition channel amplitudes D_c^i and D_c^d (where c denotes a given vibration-rotation level of the lower c state) to the body-fixed dipole transition moments $d(R)$ evaluated in Ref. [8].

Note that the K matrix thus evaluated is not symmetric by construction nor is its eigenvector matrix T exactly unitary. These properties provide a check *a posteriori* of the proper convergence of the calculation that to some extent depends on the choice of the $N_{I_o}+N_{D_o}$ solutions ψ^ρ entered into Eq. (6) as well as on the choice of the logarithmic derivatives $-b^{(x)}$ at $R=R_0$. In order to obtain a total K matrix that is energy independent over a range of, say, a few hundred reciprocal centimeter units, we have found that it is advantageous to ''artificially'' open a number of ionization channels, thereby including weakly closed channels in the reaction matrix as is customary in MQDT. These and other more technical aspects of the method will be discussed in detail in a forthcoming publication [12].

III. RESULTS

A. Details of calculation

In our calculations, we covered the range from 125 000 to 133 000 cm^{-1} (see Fig. 1). A few additional calculations in selected portions of the 118 000–125 000 cm^{-1} range will be discussed in Sec. III C below. We used the clamped-nuclei $^3\Pi_g$ and $^3\Delta_g$ quantum defects from Ref. [8] along with the $^3\Pi_u$ defect curve representing the lower state. A few calculations of upper-state continuum levels of c symmetry were also made and required in addition quantum defects for the $^3\Sigma_g{}^+$ electronic symmetry. These were taken from Ref. [13]. The number of open ionization channels $X\ ^2\Sigma_g^+, v^+, N^+, l$ to be taken into account in the range of interest varies from 2 at the lower edge up to a maximum of 15 at the upper edge depending on the $N^{c(d)}$ value considered. N here and later is the total angular momentum exclusive of spin. The superscript c or d denotes, respectively, levels with total parity $+(-1)^N$ or $-(-1)^N$ [sometimes also referred to as $(+)$ and $(-)$ Kronig parity levels]. The whole range lies above the $H(1s)+H(2s,p)$ dissociation limit at 118 375.6 cm^{-1}. There are two triplet gerade states converging to this limit, $a\ ^3\Sigma g^+$ and $i\ ^3\Pi_g$, but we have included only the latter in our calculations because, first, most of the resonances observed by Bjerre, Helm and, collaborators [5,6] are of d symmetry for which Σ^+ channels play no role anyway, and second, the dynamics in this region is expected to be dominated by the $^3\Pi_g$ and $^3\Delta_g$ symmetries as discussed in Ref. [8].

In the calculations of the total K matrix we used $R_0=7$ a.u. For each selected logarithmic derivative $-b$ at R_0 we included about 55 vibration or rotation levels associated with the $X\ ^2\Sigma_g^+\ H_2{}^+$ ground state and about 65 vibration/rotation levels associated with the $A\ ^2\Sigma_u^+$ repulsive excited core state. Thus for each selected energy and $N^{c(d)}$ value, the ''normal'' rovibronic MQDT calculation was carried out with a total of 150–250 channels depending on the parity and the energy. The calculational procedure followed exactly the method described in Ref. [13]. The number of ''artificially'' opened weakly closed channels was of the order of 20 so that the dimension of the resulting total K varied between 20 and 40.

The convergence of the calculations was ensured by accepting only K matrices for which the mean deviation of the elements of $T^{tr}T$ (T eigenvector matrix of K) from those of the unit matrix was less than 0.002 and the maximum deviation, less than 0.05 (and in general less than 0.01). In a few cases (indicated in Table I below), we have not been able to obtain satisfactory convergence in the calculations. We found that the total K matrix thus obtained for a given $N^{c(d)}$ value in general remained constant over a range of about 100 cm^{-1} so that its evaluation was required only at corresponding energy intervals.

The next step of the calculations involved the evaluation of the stationary ionization/dissociation wave functions

TABLE I. Triplet gerade resonances in H_2 (cm^{-1})

v''	$N''^{c(d)}$	$N^{c(d)}$	E(obs)[a,b]	E(calc)[a]	Obs.-calc.	Γ(obs)	Γ(calc)	Remark
7	1[d]	2[d]	125 383	125 379	+4	[29[e]],10[f]	16.8	e,f
			$v^+=1$ ionization threshold at 126 608.6					
8	1[d]	2[d]	126 764	126 762	+2	24	15.9	e
7	1[d]	2[d]	127 016.5	127 014	+3		1.8	g,h
8	1[d]	2[d]	127 015.0	127 014	+1		1.2	g,h
9	1[d]	2[d]	128 034	128 031	+3	20	15.0	e
9	1[d]	1[c]	128 324.1	128 317	+7	2	1.3	h,i
9	1[d]	2[d]	128 331.5	128 329	+3	2	1.3	h,i
			$v^+=2$ ionization threshold at 128 672.6					
9	1[d]	2[d]	129 188	129 187	+1	15	13.1	e
10	1[d]	2[d]	129 188	129 187	+1	16	13.2	e
10	1[d]	1[c]	129 199	129 198	+1	1.7	1.9	e,i
10	1[d]	2[d]	129 279	129 286	−7	2.2	1.3	e,i
10	1[d]	1[c]	130 085.0	130 094	−9	3.5	1.2	e,i,j
11	1[d]	1[c]	130 084.2	130 094	−10	4	1.2	i
11	1[d]	2[d]	130 132.4	130 138	−6	3	2.0	i,k
11	3[d]	2[d]	130 132.6	130 138	−5	2	1.5	i,k
10	1[d]	2[d]	130 133.4	130 142	−9	2.9	1.8	e,i,k
10	3[d]	2[d]	130 132.5	130 142	−9	4	1.8	e,h,k
10	1[d]	2[d]	130 228	130 226	+2	15	12.5	e
11	1[d]	2[d]	130 227	130 226	+1	15	11.6	e
10	5[d]	4[d]	130 278.4	130 279	−1	3	1.1	i,l
11	3[d]	4[d]	130 277.5	130 279	−1	2	1.0	i
10	5[d]	4[d]	130 321.6	130 327	−5	2	1.1	i
11	3[d]	4[d]	130 320.5	130 327	−6	2	1.2	i

through application of the appropriate asymptotic boundary conditions to each channel component by using standard MQDT procedures. These calculations were carried out on a fine energy mesh, typically 1 cm^{-1} or less, depending on the widths of the resonances studied. In a further step, the stationary wave functions were recombined to yield outgoing particle waves in each selected open channel, *i* or *d*. In the final step, the real channel dipole amplitudes D_c^i and D_c^d were appropriately superposed to yield the complex transition amplitude for fragmentation into each channel, and hence the corresponding partial cross section or oscillator strength.

B. Comparison with experiment

Table I collects all 18 triplet gerade excited resonances listed in Ref. [5] (their Table I) and all 23 resonances observed in Ref. [6] (their Table III). The reported transition frequencies have been converted into absolute upper-state energies by adding the appropriate $c\ ^3\Pi_u^-$, v'', N'' level energies from Ref. [8]. Note that all lower-state levels are in fact known through calculations only and therefore the upper-state energies converted from the observed transition frequencies also are affected by the error of calculation. The observed widths are also given and, for easy comparison with Refs. [5,6], the quantum numbers v'', N'' of the lower level from which a given resonance was excited is indicated in addition to the upper-state $N^{c/d}$ value. These data are compared with the results of the present calculations.

The observed and calculated resonance positions agree within a mean deviation of 7 cm^{-1}, a gratifying result considering that the present calculations are fully *ab initio* with regard to both the upper and lower levels. Also the excitation is very high, up to 1 eV above the ionization threshold. Further, all assignments v'', N'', and $N^{c(d)}$ given in Refs. [5,6] are corroborated by the present work in spite of the fact that the upper-state *N* assignments in the experimental papers were to some extent tentative. The resonances that are newly assigned in the present work are indicated.

The calculations reproduce nicely the alternation of ''broad'' and ''narrow'' resonances observed in the experiments. The agreement of the observed and calculated resonance widths is also satisfactory. Note that with few exceptions, the calculated widths are smaller than the experimental ones. This trend is most pronounced for the lowest broad resonances. The worst case is the resonance at 125 383 cm^{-1}, where $\Gamma_{calc}/\Gamma_{obs}=0.6$. According to Bjerre [14], the experiments of Refs. [5,6] systematically overestimate the resonance widths. This is due to saturation effects that affect the relative accuracy of the measured widths of broad as well as narrow resonances. These experimental difficulties appear to have been overcome in the more recent differential cross-section measurements of Siebbeles *et al.* [15] who studied four low-lying broad resonances in excitation from various *c*-state levels. One of these is the 125 383 cm^{-1} resonance for which Ref. [15] gives a value of 16 ± 1 cm^{-1} in agreement with the present calculated value of 16.8 cm^{-1} (cf.

TABLE I. (*Continued.*)

v''	$N''^{c(d)}$	$N^{c(d)}$	E(obs)[a,b]	E(calc)[a]	Obs.-calc.	Γ(obs)	Γ(calc)	Remark
			$v^+=3$ ionization threshold at 130 613.5					
11	1^d	1^c	130 862.8	130 864	−1	2	1.2	i
12	1^d	1^c	130 862.6	130 864	−1	2	1.2	i
11	1^d	1^c	130 917.6	130 907	+11	2	3.3	i,h
12	1^d	2^c	130 916.9	130 919	−2	2	4.9	i
11	1^d	2^d	130 925.1	130 931	−6	4	3.7	m
11	1^d	2^d	130 952.1	130 957	−5	4	3.8	m
12	1^d	2^d	131 045	131 045	0	<2	1.3	m
11	3^d	4^d	131 127.1	131 139	−12	3	1.6	i
11	5^d	4^d	131 128.2	131 139	−11		1.6	i
11	1^d	2^d	131 145	131 145	0	15	10.5	e
12	1^d	2^d	131 145	131 145	0	14	10	e
11	3^d	3^c	131 215			20		e,n
11	3^d	4^d	131 312	131 317	−5	45	49.1	e
12	1^d	1^c	131 604.3			3		i,o
12	1^d	2^d	131 662.0	131 681	−19	2	4.1	i,p
12	1^d	2^d	131 935	131 950	−15	11	9.5	e,p
12	1^d	1^c	132 255.3			4		i,n
12	1^d	2^d	132 307.4	132 328	−21	2	1.2	i,p
			$v^+=4$ ionization threshold at 132 435.0					
12	1^d	2^d	132 588			10		e,n

[a]Total energy above the ground level $X^1\Sigma_g^+$, $v=0$, $J=0$.

[b]Obtained from the transition energies listed in Refs. [5,6] by adding the appropriate *c*-state level energies from Ref. [8].

[c]Total parity $+(-1)^N$.

[d]Total parity $-(-1)^N$.

[e]Lembo *et al.*, Ref. [5] (Table I).

[f]From Siebbeles *et al.*, Ref. [15] (Table I). The value from Ref. [5] is given in square brackets (see the discussion in the text).

[g]Lembo *et al.*, Ref. [6] (Table I). These resonances have been observed only in ionization. They are included here in view of the following discussion; c.f. in particular Table IV.

[h]Present assignment.

[i]Lembo *et al.* [Ref. [6]] (Table III).

[j]Calculated in ionization, with negligible intensity in dissociation.

[k]According to the calculations, there are two closely spaced resonances with $N=2^d$: the first, at 130 138 cm^{-1} is strong but appears only in ionization. The second, at 130 142 cm^{-1}, is weaker and appears also in dissociation.

[l]This resonance is calculated as a window resonance appearing on top of a broad feature centered at 130 416 cm^{-1} with a width of 57 cm^{-1} that has not been reported in Ref. [6].

[m]Lembo *et al.*, Ref. [6] (Table I and II). These resonances have been observed only in ionization. They are included here in view of the following discussion; cf. in particular Fig. 3.

[n]Resonance not found in the calculations due to numerical instabilities. See, however, Table III of Ref. [8].

[o]No resonance of symmetry $N^{c(d)}=1^c$ or 2^d found in the calculations.

[p]Deviation probably related to numerical instabilities in the calculation.

Table I; two more of the resonances reported in Ref. [15] are discussed in Sec. III C below).

As already mentioned, the ''sharp'' resonances have for the most part been observed both in the photoionization and in the depletion spectra. While no quantitative information concerning the dissociation and ionization yields is given in Ref. [6], Refs. [5] and [6] each present an example of observed photoionization and depletion spectra. Figures 2 and 3 compare these observed ionization/depletion spectra with the theoretical ionization/dissociation spectra. Figure 2 illustrates one of the ''broad'' resonances observed in Ref. [5]: This resonance as well as the two much sharper features nearby, while strong in the depletion spectrum, do not appear at all in ionization. It can be seen that this behavior is perfectly reproduced by the theory that also correctly accounts for the two sharp ''parasite'' features. Reference [6] reports a spectrum containing several ''sharp'' resonances with varying ratios of the ionization and dissociation yields. This is illustrated by Fig. 3. The observed and calculated photoionization spectra are again in quite good agreement with regard

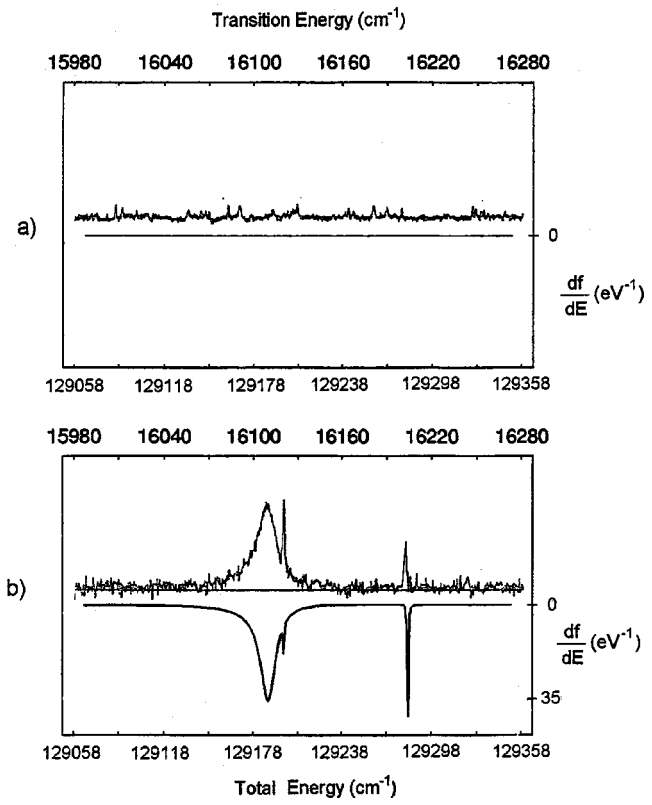

FIG. 2. Example of a ''broad'' predissociation resonance. (a) Observed and calculated in ionization, (b) observed in depletion and calculated in dissociation (c.f. the text). The lower state is the $v=10$, $N=1$ level of $c\ ^3\Pi_u^-$. The intensity scale of the theoretical spectra corresponds to the calculated oscillator strength distribution (df/dE in units eV^{-1}).

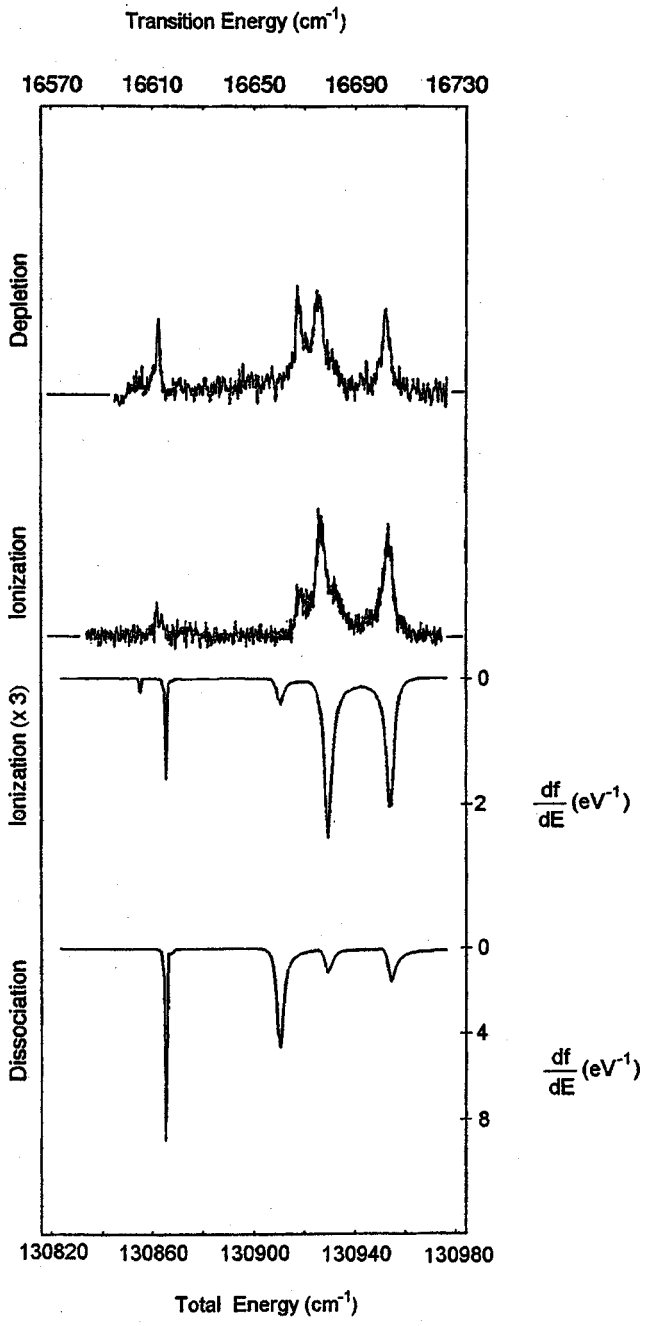

FIG. 3. Example of ''narrow'' predissociation/preionization resonances. The lower state is the $v=11$, $N=1$ level of $c\ ^3\Pi_u^-$. Top: observed depletion and ionization spectra. Bottom: calculated ionization and dissociation spectra. The intensity scale of the theoretical spectra corresponds to the calculated oscillator strength distribution (df/dE in units eV^{-1}). See the text for details.

to positions, relative intensities, and widths. Two of the resonances appear enhanced in the depletion spectrum with respect to the other two, indicating that they are more strongly predissociated. It can be seen that theory indeed correctly predicts the same pair of resonances to be strongest in the dissociation spectrum. Note that a different oscillator strength scale was used for the two theoretical spectra in Fig. 3 to facilitate comparison with the experimental spectra. In particular, we reduced the plotting scale of the calculated dissociation spectrum of Fig. 3 by a factor of 3 with respect to the ionization spectrum. Bjerre [14] asserts that judging from the way the experiments were done, this factor must be >1 because in the depletion spectra the molecular beam and two laser beams must be spatially superposed, whereas the ionization spectrum is obtained by superposition of the molecular beam with just one laser beam. Somewhat more intuitively, it appears [14] that if this factor was $\gg 1$, one would probably not observe a depletion spectrum at all. Therefore, the adjustment factor 3 determined here appears reasonable.

C. Analysis of fragmentation mechanisms

The results presented in the preceding subsection illustrate the power of the *ab initio* MQDT approach employed here. It is tempting to get more detailed insight into the physical mechanisms at work by examining the composition of the multichannel wave functions.

Table II collects information on the spectral composition of the wave functions evaluated for the ''broad'' resonances with $N^{c(d)}=2^d$. For each resonance, we give the position and width as well as the dominant closed-channel contributions. Each such channel is denoted by $l(\nu)$, v^+, N^+. v^+, N^+ and

TABLE II. ''Broad'' resonances with $N=2$[d] in the range 125 000–132 000 cm^{-1}. Energies and widths in cm^{-1}.

Energy				Width		
BO[b]	Obs.-calc.	MQDT	Obs.-calc.	BO[c]	MQDT	Dominant bound channels[a]
125 349	+34	125 379	+4	18	16.8	$l=2,\ \nu=3.04,\ v^+=7,\ N^+=1$
						$l=2,\ \nu=3.02,\ v^+=7,\ N^+=3$
126 734	+30	126 762	+2	16	15.9	$l=2,\ \nu=3.04,\ v^+=8,\ N^+=1$
						$l=2,\ \nu=3.02,\ v^+=8,\ N^+=3$
128 007	+27	128 031	+3	14	15.2	$l=2,\ \nu=3.05,\ v^+=9,\ N^+=1$
						$l=2,\ \nu=3.02,\ v^+=9,\ N^+=3$
129 166	+22	129 187	+1	13	13.2	$l=2,\ \nu=3.05,\ v^+=10,\ N^+=1$
						$l=2,\ \nu=3.03,\ v^+=10,\ N^+=3$
130 207	+21	130 226	+2	11	13.2	$l=2,\ \nu=3.05,\ v^+=11,\ N^+=1$
						$l=2,\ \nu=3.03,\ v^+=11,\ N^+=3$
131 128	+17	131 145	0	10	10.5	$l=2,\ \nu=3.05,\ v^+=12,\ N^+=1$
						$l=2,\ \nu=3.03,\ v^+=12,\ N^+=3$
131 922	+13	131 950	−15	8	9.5	$l=2,\ \nu=3.05,\ v^+=13,\ N^+=1$
						$l=2,\ \nu=3.03,\ v^+=13,\ N^+=3$
						$l=2,\ \nu=11.98,\ v^+=4,\ N^+=3$
						$l=2,\ \nu=7.00,\ v^+=5,\ N^+=1$

[a]cf. the text.
[b]Calculated [5] in the Born-Oppenheimer approximation. The *ab initio* Born-Oppenheimer potential-energy curve was shifted so as to correlate correctly with the $n=3$ threshold at 133 608.8 cm^{-1}.
[c]Calculated in Ref. [5] in the pure precession approximation using the Fermi golden rule (see the text).

l are the vibrational and rotational quantum numbers of the ground-state ion core and the Rydberg electron orbital quantum number as before. ν is the effective principal quantum number for each channel, given in parenthesis and evaluated with the resonance energy E and the threshold energy E^+ according to $E-E^+=-\mathcal{R}/\nu^2$, where $\mathcal{R}$ is the Rydberg energy. Inspection of Table II suggests immediately that the series of broad resonances corresponds to a vibrational progression associated with a *d* electron. The effective principal quantum number, roughly constant along the series, is about 3.03, i.e., $n=3,\mu=-0.03$. This quantum-defect value corresponds to $\mu_{dd}^{(\Delta)}$ near $R\approx 3$ as can be seen with reference to Fig. 2(c) of Ref. [8]. It thus follows that the series of broad resonances ''belongs'' to the $j^3\Delta_g^-$ state as had indeed been concluded already by Lembo *et al.* [5].

Table II also lists the Born-Oppenheimer bound vibrational levels calculated for the *j* state with the *ab initio* potential curve of Rychlewski [7,5]. The assignments in Ref. [5] were based on these theoretical Born-Oppenheimer levels. Essentially the same potential curve was used in Ref. [8] to determine the clamped-nuclei quantum-defects curve $\mu^{\Delta}{}_{dd}(R)$. The difference between the Born-Oppenheimer

TABLE III. Resonances with $N=2$[d] in the range 118 000–125 000 cm^{-1}. Energies and widths in cm^{-1}.

Total Energy			Width			
E(calc)[b]	E(obs)	Obs.-calc.	Γ(calc)[b]	Γ(obs)	Experiment	Dominant bound channels[a]
118 734	118 725.16	−9	1.1		[c]	$l=2,\ \nu=3.03,\ v^+=3,\ N^+=1,3$
120 553	120 555.6	+3	1.2		[d]	$l=2,\ \nu=3.03,\ v^+=4,\ N^+=1,3$
	120 552	−1		<1	[e]	
122 281	122 279	−2	25.4	23±1	[f]	$l=2,\ \nu=3.03,\ v^+=5,\ N^+=1,3$
	122 281	0		[50±10]	[e]	
123 883	123 887	+4	18.0	19±1	[f]	$l=2,\ \nu=3.04,\ v^+=6,\ N^+=1,3$
	123 882	−1		[50±10]	[e]	

[a]c.f. the text.
[b]MQDT, present work.
[c]Jozefowski *et al.*, Ref [19].
[d]Koot *et al.*, Ref. [17].
[e]de Bruijn *et al.*, Ref. [18].
[f]Siebbeles *et al.*, Ref. [15].

levels and our calculated resonance positions is due to the adiabatic and nonadiabatic effects that are taken into account in our approach but were neglected in Refs. [5,7]. Table II further lists the *j*-state resonance widths calculated in Ref. [5] using the Fermi golden rule and assuming a rotational-electronic Coriolis interaction between the $j\ ^3\Delta_g$ and the $i\ ^3\Pi_g$ state. The predissociating interaction is then given by the familar *l*-uncoupling matrix element

$$V_E = -[N(N+1)-2]^{1/2}\langle i\ ^3\Pi_g|l_-|j\ ^3\Delta_g\rangle \times\left\langle \chi_E^{(^3\Pi_g)}(R)\left|\frac{1}{\mu R^2}\right|\chi_v^{(^3\Delta_g)}(R)\right\rangle, \quad (7)$$

where l_- is the orbital angular momentum lowering operator component, χ_E and χ_v are continuum and bound vibrational wave functions, respectively, and where the electronic matrix element may be evaluated in the ''pure precession'' approximation by assuming $l=2$ [16]. It is interesting to see that the Fermi golden rule expression and MQDT predict very similar predissociation widths in this particular instance. This indicates that the *j* state, by contrast to the *r* state (see below), is only little affected by multichannel interactions.

Table III lists a few additional *j*-state resonance positions and widths ($v=3-6$, not included in Table I) that lie below the ionization threshold but above the $H(1s)+H(n=2)$ dissociation limit and have been observed by fast-beam photofragment spectroscopy by Siebbeles *et al.* [15], Koot *et al.* [17] and de Bruijn and Helm [18]. The very lowest of these are quite narrow because they lie below the potential hump of the $i\ ^3\Pi_g$ state (see Fig. 1) and therefore predissociate by tunneling through that hump. The observed dramatic increase of the predissociation width between $v=4$ and $v=5$ is correctly reproduced by MQDT. The widths determined in Ref. [15] are in much better agreement with theory than those determined in Ref. [18]. The reason is presumably again that the determinations of Ref. [18] are affected by saturation effects while those of Ref. [15] are not (see the discussion in Sec. III B).

Table IV is analogous to Table II and presents the eigenvector analysis for the series of ''sharp'' resonances corresponding to $N^{c(d)}=2^d$. The situation here appears at first more confusing since each resonant state is spread over a whole range of equally dominant v^+ and hence ν values, the latter ranging from $v\approx 3$ up to 4 (with a component $\nu\approx 7$ also appearing in two instances). We know that generally speaking levels with lower v^+ or higher ν tend to preionize more easily, while levels with higher v^+ or lower ν tend to predissociate: In other words, the amount of energy exchanged between the vibrational and electronic degrees of freedom tends to be minimized. This type of ''energy gap law'' (or propensity rule) has been discussed, e.g., in Ref. [20]. The larger spread of v^+ channel components seen in Table IV as compared to Table II thus explains why the ''sharp'' resonances have a better chance to preionize *and* predissociate, and therefore to be observed in the photoioization as well as in the depletion spectrum.

TABLE IV. ''Sharp'' resonances with $N=2^d$.

Energy[a]	Width[a]	Series	Dominant bound channels[b]
127 014[c]	1.8	$\nu\approx n.85$:	$l=2,\ \nu=3.91,\ v^+=5,\ N^+=1$
		$\nu\approx n.85$:	$l=2,\ \nu=3.85,\ v^+=5,\ N^+=3$
		$\nu\approx n.85$:	$l=2,\ \nu=2.90,\ v^+=9,\ N^+=3$
128 329	1.3	$\nu\approx n.85$:	$l=2,\ \nu=3.84,\ v^+=6,\ N^+=1$
		$\nu\approx n.85$:	$l=2,\ \nu=3.79,\ v^+=6,\ N^+=3$
		$\nu\approx n.14$:	$l=2,\ \nu=3.24,\ v^+=8,\ N^+=3$
		$\nu\approx n.03$:	$l=2,\ \nu=3.06,\ v^+=9,\ N^+=3$
129 286	1.3	$\nu\approx n.03$:	$l=2,\ \nu=4.05,\ v^+=6,\ N^+=3$
		$\nu\approx n.85$:	$l=2,\ \nu=3.67,\ v^+=7,\ N^+=3$
		$\nu\approx n.33$:	$l=2,\ \nu=3.40,\ v^+=8,\ N^+=3$
		$\nu\approx n.14$:	$l=2,\ \nu=3.22,\ v^+=9,\ N^+=1$
		$\nu\approx n.14$:	$l=2,\ \nu=3.20,\ v^+=9,\ N^+=3$
		$\nu\approx n.03$:	$l=2,\ \nu=3.04,\ v^+=10,\ N^+=3$
130 142	1.5	$\nu\approx n.85$:	$l=2,\ \nu=2.93,\ v^+=7,\ N^+=1$
		$\nu\approx n.85$:	$l=2,\ \nu=3.88,\ v^+=7,\ N^+=3$
		$\nu\approx n.33$:	$l=2,\ \nu=3.33,\ v^+=9,\ N^+=3$
		$\nu\approx n.14$:	$l=2,\ \nu=3.18,\ v^+=10,\ N^+=1$
		$\nu\approx n.14$:	$l=2,\ \nu=3.16,\ v^+=10,\ N^+=3$
		$\nu\approx n.03$:	$l=2,\ \nu=3.04,\ v^+=11,\ N^+=1$
		$\nu\approx n.03$:	$l=2,\ \nu=3.02,\ v^+=10,\ N^+=3$
130 931	3.7	$\nu\approx n.85$:	$l=2,\ \nu=7.85,\ v^+=4,\ N^+=3$
		$\nu\approx n.14$:	$l=2,\ \nu=4.11,\ v^+=7,\ N^+=3$
		$\nu\approx n.33$:	$l=2,\ \nu=3.28,\ v^+=10,\ N^+=3$
		$\nu\approx n.14$:	$l=2,\ \nu=3.14,\ v^+=11,\ N^+=1$
		$\nu\approx n.14$:	$l=2,\ \nu=3.12,\ v^+=11,\ N^+=3$
		$\nu\approx n.03$:	$l=2,\ \nu=3.01,\ v^+=12,\ N^+=3$
130 957	3.8	$\nu\approx n.85$:	$l=2,\ \nu=7.91,\ v^+=4,\ N^+=3$
		$\nu\approx n.14$:	$l=2,\ \nu=4.11,\ v^+=7,\ N^+=3$
		$\nu\approx n.85$:	$l=2,\ \nu=3.74,\ v^+=8,\ N^+=3$
		$\nu\approx n.33$:	$l=2,\ \nu=3.28,\ v^+=10,\ N^+=3$
		$\nu\approx n.14$:	$l=2,\ \nu=3.14,\ v^+=11,\ N^+=1$
		$\nu\approx n.14$:	$l=2,\ \nu=3.12,\ v^+=11,\ N^+=3$
		$\nu\approx n.03$:	$l=2,\ \nu=3.01,\ v^+=12,\ N^+=3$
131 045	1.5	$\nu\approx n.85$:	$l=2,\ \nu=5.72,\ v^+=5,\ N^+=3$
		$\nu\approx n.85$:	$l=2,\ \nu=4.82,\ v^+=6,\ N^+=1$
		$\nu\approx n.33$:	$l=2,\ \nu=4.72,\ v^+=6,\ N^+=3$
		$\nu\approx n.85$:	$l=2,\ \nu=3.76,\ v^+=8,\ N^+=3$
		$\nu\approx n.14$:	$l=2,\ \nu=3.14,\ v^+=11,\ N^+=3$

[a]Present calculated values in cm^{-1}.

[b]cf. the text.

[c]Experimentally observed only in ionization.

A closer inspection of Table IV reveals that within the spread of effective principal quantum number values recurring subgroups with roughly constant ν appear: ≈ 3.85, ≈ 3.33, ≈ 3.14, and ≈ 3.03. The latter value is again characteristic for the $j\ ^3\Delta_g$ state, while the former values characterize the $r\ ^3\Pi_g$ state in the range from $R=3-6$: as seen in Fig. 1, the *r* state starts out at small *R* as a $1\sigma_g 4d\pi$ state and evolves adiabatically to $1\sigma_g 3d\pi$ and eventually to the $n=3$ dissociation limit through interaction with the doubly excited $1\sigma_u 2p\pi_u$ repulsive state (cf. the detailed discussion in Ref. [8]). Its effective quantum number stays very near $n=4$ up to $R\approx 3$ and then begins to decrease rapidly: $\nu=3.8$ for $R=3.5$, $\nu=3.3$ near $R=4$, $\nu=3.2$ for $R=5$. The

''sharp'' series of resonances thus corresponds to vibrational wave functions largely confined to the region between $R=3$ and 5. Figure 1 suggests that this confinement arises because the vibrational motion takes place in an effective potential well whose left limb is formed by the diabatic doubly excited $1\sigma_u 2p\pi_u$ repulsive state and whose right limb corresponds to the singly excited $1\sigma_g 3d\pi_g$ configuration converging toward the $n=3$ dissociation limit. [The left limb formed by the doubly excited $1\sigma_u 2p\pi_u$ repulsive state is not shown in the figure but can be imagined easily as rising from the $n=2$ (i state) asymptote toward the left and passing into the ionization continuum near about $R=3.5$ a.u.]

Note finally that the above interpretation is in apparent contradiction with the r-state assignments given in Table III of Ref. [8] which in part are based on the same resonances listed in Table IV, but which were calculated as bound states (neglecting the discrete-continuum couplings). We stress here once again that we have here a situation where strongly avoided crossings occur, as illustrated by Fig. 1, and therefore apparently conflicting interpretations are possible depending on the way the calculations are made and analyzed. The main point of course is that we are in a position to carry out quantitative calculations that are independent of the interpretative point of view adopted.

IV. CONCLUSION

In this paper, we have extended the analysis of triplet bound states of H_2 presented by Ross *et al.* [8] to the energy range above the ionization threshold. The intermediate region between the $n=2$ dissociation threshold and the I.P. remains to be studied theoretically in more detail, although in Sec. III C we have discussed some of the fast-beam photofragment spectroscopic results of Siebbeles *et al.* [15] de Bruijn and Helm [18] pertaining to this range.

The present analysis of decay processes in highly excited triplet gerade H_2 accounts for rather diverse intramolecular interactions in a single unified approach: At the lower edge of the energy range studied here, the vibration/rotation levels of the $j\ ^3\Delta_g^-$ state are coupled by rotational-electronic Coriolis interaction to bound levels of the $i\ ^3\Pi_g^-$ state that in turn mediate the slow dissociation by tunneling through the potential barrier of this state (accidental predissociation). At higher energy, the $j\approx i$ Coriolis interaction leads to fast dissociation directly into the vibrational continuum of the i state. The $r\ ^3\Pi_g$ state undergoes strong electronic mixing with the antibonding doubly excited $1\sigma_u 2p\pi_u$ configuration, and its potential-energy curve thereby acquires the shape of a ''shelf'' state. We have shown that it is this strongly mixed nature that allows the levels of this state to simultaneously predissociate and preionize. At the same time, rotational-electronic Cariolis coupling $r\approx j$ is also active (cf. Table IV): Note that the ''pure precession'' approximation would restrict this coupling to the $i\approx j$ pair of states. The electronic interaction between singly and doubly excited configurations is so strong that the adiabatic picture of noncrossing mixed curves appears to be the better starting point for an understanding of the fragmentation dynamics than would be the diabatic crossing curves corresponding to ''pure'' singly or doubly excited states. The surprisingly small observed and calculated level widths for ionization and dissociation point in this direction. At the same time, we have found that the vibrational motion in the observed r state resonances appears to be effectively confined to a small range of R values, between about 3 and 5 a.u. This phenomenon in turn is best rationalized in terms of single-configuration potential curves. The main message here of course is that our *ab initio* MQDT approach handles all these complexities in a global fashion without requiring a special provision for each particular effect. We believe that our approach will also be required to treat the fragmentation dynamics in alkali dimers where highly excited states play a role in the formation of ultracold molecules.

ACKNOWLEDGMENTS

Dr. E. Reinhold (University of Amsterdam) is thanked for his help at the early stage of the calculations. S.C.R. acknowledges the support of the Natural Sciences and Engineering Research Council of Canada.

[1] O. W. Richardson, *Molecular Hydrogen and its Spectrum* (Yale University Press, New Haven, CT, 1934).
[2] H. M. Crosswhite, *The Hydrogen Molecule Wavelength Tables of Gerhard Heinrich Dieke* (Wiley-Interscience, New York, 1972).
[3] E. E. Eyler and F. M. Pipkin, Phys. Rev. A **27**, 2462 (1983).
[4] N. Bjerre, S. R. Keiding, L. J. Lembo, and H. Helm, Phys. Rev. Lett. **60**, 2465 (1988).
[5] L. J. Lembo, D. L. Huestis, S. R. Keiding, N. Bjerre, and H. Helm, Phys. Rev. A **38**, 3447 (1988).
[6] L. J. Lembo, N. Bjerre, D. L. Huestis, and H. Helm, J. Chem. Phys. **92**, 2219 (1990).
[7] J. Rychlewski, J. Mol. Spectrosc. **104**, 253 (1984). See also Ref. [5].
[8] S. C. Ross, Ch. Jungen, and A. Matzkin, Can. J. Phys. (to be published).
[9] A. Matzkin, Phys. Rev. A **59**, 2043 (1999).
[10] Ch. Jungen and S. C. Ross, Phys. Rev. A **55**, R2503 (1997).
[11] *Molecular Applications of Quantum Defect Theory*, edited by Ch. Jungen (Institute of Physics, Bristol, 1996).
[12] Ch. Jungen and S. C. Ross (unpublished).
[13] S. C. Ross and Ch. Jungen, Phys. Rev. A **49**, 4353 (1994); **49**, 4364 (1994) (reprinted in Ref. [11]).
[14] N. Bjerre (private communication).
[15] L. D. A. Siebbeles, J. M. Schins, J. Los, and M. Glass-Maujean, Phys. Rev. A **44**, 1584 (1991).
[16] J. H. van Vleck, Phys. Rev. **33**, 467 (1929).
[17] W. Koot, W. J. van der Zande, J. Los, S. R. Keiding, and N. Bjerre, Phys. Rev. A **39**, 590 (1989).
[18] D. P. de Bruijn and H. Helm, Phys. Rev. A **34**, 3855 (1986).
[19] L. Jozefowski, Ch. Ottinger, and T. Rox, J. Mol. Spectrosc. **183**, 381 (1994).
[20] C. H. Greene and Ch. Jungen, Adv. At. Mol. Phys. **21**, 51 (1985).